Magazine of Civil Engineering

ISSN 2712-8172

journal homepage: http://engstroy.spbstu.ru/

Research article

UDC 624.13

DOI: 10.34910/MCE.125.6

Numerical analysis of rainfall-induced slope instability using a reduced-scale model

F. Hamrouni [1], ***M. Jamei*** [2] ✉, ***Y. Alassaf*** [2]

[1] *Tunis El Manar University, National Engineering School of Tunis, Civil Engineering Laboratory, Tunis, Tunisia*

[2] *Northern Border University, Arar, Saudi Arabia*

✉ *mehjamei@yahoo.fr*

Keywords: climate changes, landslide, rainfall, finite element modeling, unsaturated soil, physical model

Abstract. The climatic changes induce now more and more serious environmental problems such as landslides, especially in arid and semi-arid countries where rainfalls happen with high and short duration intensity. This paper aims to study the influence of unsaturated mechanical properties on the slope instability. The research was conducted based on the combination of a physical model and numerical simulations with the aim to analyze rainfall-induced slope failure. The benefits of the proposed method are: 1) increase of monitoring efficiency by considering several parameters in large ranges of variation; 2) cost reduction by a combination of minimal laboratory physical model data and numerical modeling. In this study, the effect of rainfall intensity and duration as a hydraulic loading was investigated. The used model is an elastoplastic one based on effective stresses and a non-associative flow rule. A function of a reduction of mechanical parameters with suction was implemented in CODE_BRIGHT software. The results are presented in terms of: 1) displacement values; 2) evolution of pore water pressure (PWP); 3) plastic deviatory strains and saturation zones.

Funding: The authors extend their appreciation to the Deanship of Scientific Research at Northern Border University, Arar, Saudi Arabia, for funding this research work through the project number “NBU-FFR-2024-2740-01“.

Citation: Hamrouni, F., Jamei, M., Alassaf, Y. Numerical analysis of rainfall-induced slope instability using a reduced-scale model. Magazine of Civil Engineering. 2024. 17(1). Article no. 12506. DOI: 10.34910/MCE.125.6

1. Introduction

Weathered shallow landslides have been observed in different regions in the world. In fact, climatic changes have led to many extreme weathering scenarios. Among them, the rainfalls which are more and more intensive and happen in a short duration, causing different environmental hazards such as landslides. Serious landslides have often occurred during or just after rainfall (a non-exhaustive example of disaster has occurred in the North West of Tunisia (Béja) [1, 2]). So, the objective of this study is to provide an expertise methodology, based on the consideration of the hydro-mechanical coupling for unsaturated soils. This expertise aims to: 1) provide a power modeling tool to reproduce some experimental results [1, 2]; 2) to evaluate the role of the main physical and hydraulic parameters (grain size distribution, density or porosity, saturated permeability) to explore how landslides occur and the shear band develops; 3) to inform about the influence of such numerical parameters as the mesh elements and the test of convergence.

Currently, to investigate the effects of the water pressure increase due to the rainfall water infiltration, various theoretical and numerical methods have been used. The limit analysis approach and the elastoplastic model using the so-called c-phi reduction method have been frequently used in the

engineering field. However, these approaches do not explicitly include the hydraulic-mechanical coupling stresses. Thus, in the last two decades, numerous studies have proposed several approaches considering hydraulic-mechanical coupling, which have provided a powerful tool for the prediction of the rainfall-induced landslide [2, 11]. Other researches have been also proposed to combine the modeling and field monitoring to evaluate the landslide risk [12].

In fact, some of the previously coupling approaches have considered the dependence of apparent cohesion, effective stress and friction angle with suction (and eventually the degree of saturation as function of void ratio), as well as the variation of permeability with the suction [2, 8, 9, 13]. Other approaches consider the suction or the degree of saturation as a state variable [8]. In addition, many rainfall-induced slope instability studies have focused on the role of the water retention properties under diverse rainfall scenarios on unsaturated slope stabilities [14, 17].

As noticed by experimental results, the increase of water table level is one of the most relevant conditions to landslide incidence [18–20]. The shear band, defined as a band where plastic shear strain is well developed in relation with the pore water pressure increase, which in the end, governs the failure mode. In order to deeply understand the mechanisms of such rainfall-induced failure, the study of coupling problems is now becoming an absolute need in the environmental engineering field. In this context, different reduced-scale slope models were developed to investigate the main conditions that cause slope failure and quantify the main factors that govern it under rainwater infiltration, particularly in extreme weather conditions, and under hydraulic and environmental cycles effects [20, 29].

Relevance of this study lies in the quantification, separately, of the unsaturated hydraulic parameters (unsaturated permeability and water retention function) and mechanical parameters leading to slope failure considering numerous types of soils. This study detailed the observations of the failure process, duration of soil moisture content development and pore-water pressure during the rainfall period. A pre-failure stage analysis was performed by plastic strain development. The CODE_BRIGHT program [30] was used, where the proposed model was implemented [18].

Indeed, the proposed model was based on the extension of effective stress concept to unsaturated soils, considering the cohesion reduction under humidification [8, 31, 33] (e.g., the reduction of the suction as an internal variable in the model).

The obtained numerical results show that for the long rainfall duration and for the well permeable soil, infiltration develops groundwater table from the bottom up, leading to matric suction loss in the transient unsaturated to saturated zone. Analysis of the strain evolution indicates that failure localization originates in the lower part and the shear zone develops through the superficial part to the upper part of the slope. The suction loss and the increase of the pore water pressure in the saturated zone, near the toe of the slope, are considered as the main factors leading to the slope failure.

2. Methods

2.1. The proposed hydro-mechanical model

As it is mentioned above, landslides may occur due to rapid reduction of suction under rainwater infiltration [3, 23, 34]. Obviously, experimental efforts are yet needed to link the mechanical parameters as stiffness, compressibility, cohesion and friction angle to the water content/degree of saturation and suction evolution and consider this issue in landslide analysis. For some authors, adding to the internal variables such the elastic and plastic deformation, the degree of saturation is considered as an internal variable [8]. This idea was firstly proposed by [31], and was open to debate based on experimental and theoretical evidence. At the first stage, various shear test results showed the influence of water content on friction and cohesion due to wetting-drying cycles [35, 36]. These tests highlighted the fact that the increase of water content (or saturation degree) has led to a decrease of the suction in the soil and consequently, the decrease of “apparent” cohesion and then the decrease of effective stresses. Obviously, the decrease of these mechanical parameters entailed a reduction in the soil shear strength.

In this paper, an elastoplastic model is proposed and formulated in an elastic and visco-plastic framework. A modified Mohr–Coulomb model based on effective stress (using an extended mathematical relation of [32]) has been proposed and implemented in the CODE_BRIGHT software. The algorithm of the resolution of the obtained iterative non-linear equations system was solved using a regularization method [18]. To find different previous forms of extended effective stresses formula, see, e.g. [33, 37, 39].

The suggested model defined the apparent cohesion as a nonlinear function of suction, thus leading to a non-linear shear strength-suction relationship [40].

We use here some results of triaxial drained tests conducted by [20], on the Kumano silty sand with initial relative densities (D_r varied from 58 % to 86 %). The soil was used in a physical slope model. These tests showed a Young modulus dependency on suction, which varied in the range of 3–10 MPa.

The equations of the proposed model were implemented in the CODE_BRIGHT software. Table 1 and Table 2 summarize the mechanical and hydraulic equations (for more details about the implementation of hydro-mechanical model and the applied regularization method, see, e.g. [17, 18, 39]).

Table 1. Mechanical equations used in the model.

Mechanical part of the model		
Balance equations (the variable is the effective stress tensor of water pressure)	$Div(\sigma') = \underset{\sim}{\gamma} - Grad(u_w)$	$Div(.)$ and $grad(.)$ are respectively the divergence and gradient operators. $\underset{\sim}{\gamma}$ is the vertical volumetric force (vertical unit weight force)
The effective strain rate	$\dot{\varepsilon} = \frac{d\varepsilon}{dt} = \frac{d\varepsilon^e}{dt} + \frac{d\varepsilon^p}{dt}$ $\frac{d\varepsilon^e}{dt} = \underline{\underline{A}} : \frac{d\sigma'}{dt}$	ε^e and ε^p are respectively the elastic and plastic components of an effective strain tensor. Hooke's law was used to link the elastic tensor's components to the effective stress components. σ' is effective stress, $\underline{\underline{A}}$ is the behavior tensor with components depending on the stiffness E *(function of suction)* and Poisson's ratio ν (*not dependent on the suction*).
Plastic effective deformation (determined using a non-associative flow law)	$\frac{d\varepsilon^p}{dt} = \Gamma_0 \langle \Phi(F) \rangle \frac{\partial G}{\partial \sigma'}$	Γ_0 (s^{-1}) is a fluidity parameter, F (MPa) is the yield function (Here is the Mohr–Coulomb function), G (MPa) is the plastic potential, Φ is a stress function.
The stress function	$\langle \Phi(F) \rangle = \begin{cases} 0 & \text{if} \Phi(F) < \\ \Phi(F) = F^m & \text{if} \Phi(F) > \end{cases}$	m is a parameter which depends on the material. It is experimentally calibrated. For instance, m was calibrated by some primarily numerical tests and fixed at 3 (this calibration was convenient for the studied sandy soil which exhibited dilatancy).
The yield function (F) and the visco-plastic potential (G)	$F + c'\beta = q - \delta p'$, $G + c'\beta = q - \alpha\delta p'$	α is a parameter to define non-associative plasticity rules. where $\delta = \frac{6\sin\phi'}{3-\sin\phi'}$ and $\beta = \frac{6\cos\phi'}{3-\sin\phi'}$
The first and second invariants p and q	$p = \frac{1}{3}(\sigma'_x + \sigma'_y + \sigma'_z)$ $q = \frac{1}{\sqrt{2}}\sqrt{(\sigma_x - \sigma_y)^2 + (\sigma_y - \sigma_z)^2 + (\sigma_z - \sigma_x)^2 + 6(\tau_{xy}^2 + \tau_{yz}^2 + \tau_{zx}^2)}$	c' is the effective cohesion and ϕ' is the effective friction angle.
The effective stress	$\sigma_{ij}' = \sigma_{ij} - u_a\delta_{ij} + \chi(u_a - u_w)\delta_{ij}$ The general expression of the adapted cohesion is as follows $c = c' + (u_a - u_w)\tan\phi' \left(1 + \left(\frac{u_a - u_w}{P_0}\right)^{\frac{1}{1-\lambda}}\right)^{-\lambda}$	δ_{ij} is the Kroemer's symbol ($\delta_{ij} = 1$ if $i = j$; $\delta_{ij} = 0$ if $i \neq j$)

2.2. Hydraulic constitutive models

For numerical simulations, the needed hydraulic properties are the soil-water retention curve, the relative permeability variation with suction or degree of saturation and the variation of intrinsic permeability with porosity. The following table presents all the used functions (The relative permeability function [41], van Genuchten equation fitting the water retention curve [42] and the effective saturation S_e is defined by Mualem [43]).

Fig. 1 and 2 give respectively an example of experimental calibration of water retention function and intrinsic permeability.

Table 2. Hydraulic constitutive equations.

The flow motion Richards equation	$q_w = -\frac{kk_{rw}}{\mu_w}\left(\nabla u_w + \rho_w g \nabla z\right)$	q_w (m/s) is the flux of the water, and ∇u_w is the pressure gradient vector (Pa/m). K (m/s) represents the hydraulic conductivity, k (m²) the intrinsic permeability, ρ_w (kg/m³) the water density (ρ_w =10³ kg/m³), g (m/s²) the acceleration of gravity and μ_w (Pa.s) the dynamic viscosity of water (μ_w = 10⁻³ Pa.s). These parameters are fixed for a temperature T = 20º.
The relative permeability function	$k_{rw} = S_e^{\xi}$	S_e is the effective saturation. For numerical simulation ξ = 3.
And the intrinsic permeability	$k = k_o \frac{n^3}{(1-n)^2}\frac{(1-n_o)^2}{n_o^3}$	n_o is the initial porosity and k_o is the saturated permeability corresponding to n_o. (For the calibrated experimental data, k_o = 1.8 10⁻¹¹ m² and n_o = 0.471).
Van Genuchten equation fitting the water retention curve	$S_e = \left(1+\left(\frac{u_a - u_w}{P_0}\right)^{\frac{1}{1-\lambda}}\right)^{-\lambda}$ $S_e = \frac{S_r - S_{r\min}}{S_{r\max} - S_{r\min}}$	S_r is the saturation degree, $S_{r\,\max}$ and $S_{r\,\min}$ denotes respectively the maximum and the residual saturation degree, λ and P_0 are respectively the van Genuchten parameters (P_0 is a reference capillary pressure and λ is a shape's curve), (for the calibrated experimental data, λ = 0.4, P_0 = 4 10⁻⁴ MPa, $S_{r\,\max}$ = 1 and $S_{r\,\min}$ = 0.22).

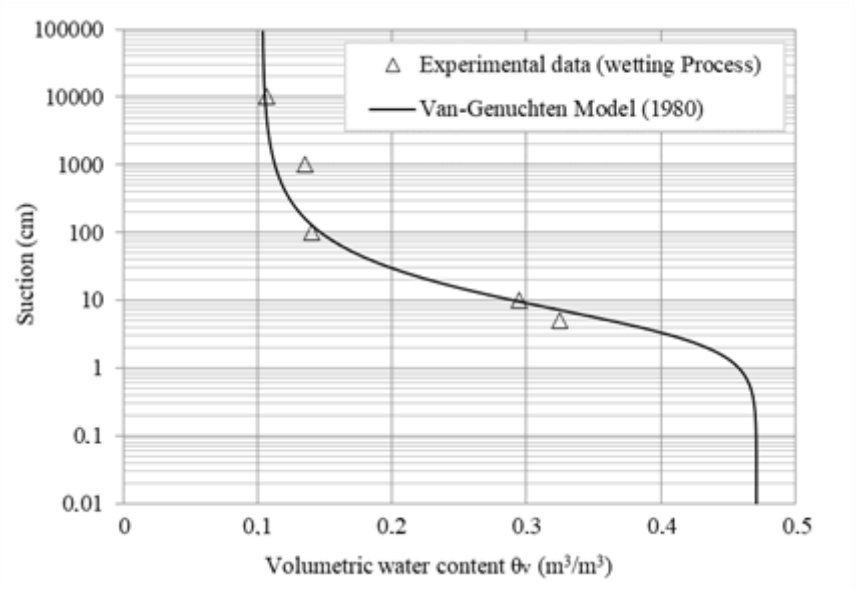

Figure 1. Fitting of water retention curve with experimental data [18].

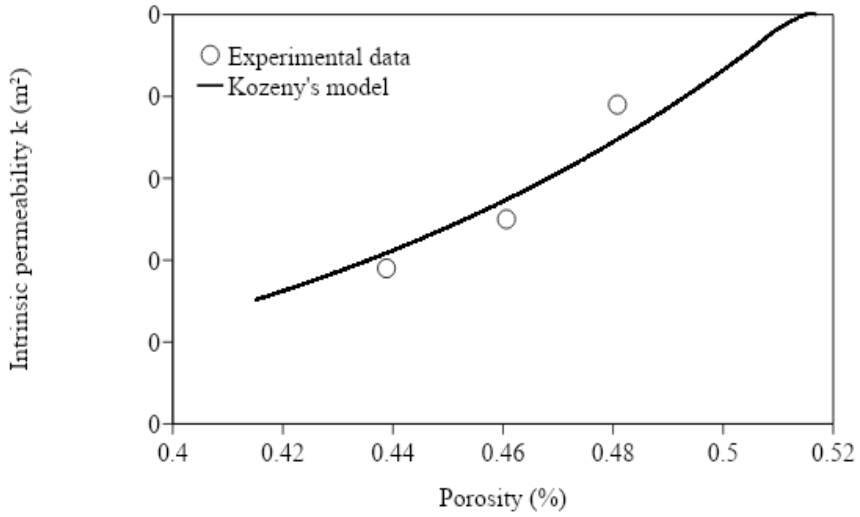

Figure 2. Saturated permeability as function of porosity for a silty sandy soil [18].

In the same context, Table 3 summarizes the modeling parameters values used in the simulations.

Table 3. Constitutive parameters.

ELASTICITY		
Parameters	Value	Parameters definition
E (MPa)	10	Young's modulus
v	0.3	Poisson's Ratio
VISCO-PLASTICITY PARAMETERS		
Parameters	Value	Parameters' definition
m	3	Stress power
Γ_o (s^{-1})	1.10^6	Viscosity coefficient (a high value is needed to approach the plastic behavior)
Q (J mol^{-1})	0.0	Parameter for temperature dependency
c'	0.0	
$tan\ \phi'$	0.4762	Total cohesion
λ	0.4	$c = c' + (u_a - u_w)\tan\phi' \left(1 + \left(\frac{u_a - u_w}{P_0} \right)^{\frac{1}{1-\lambda}} \right)^{-\lambda}$
P_0	4.10^{-4}	
α	1.10^{-4}	Parameter to reduce dilatancy: a low value for the sandy soil case (which can exhibit dilatancy)
δ	1.462	$\delta = \frac{6\sin\phi'}{3 - \sin\phi'}$

3. Results and Discussion

We employed the finite element code (CODE_BRIGHT) to build the geometry of the slope model, and used GiD pre- and post-processor [30, 44]. The slope's angle was 40 degrees. As indicated in Fig. 3 for the finite element mesh, the elements were of a four-node quadrilateral type. The numerical simulation was performed by taking into account the hydraulic and mechanical boundary conditions of the flow as shown in Fig. 3.

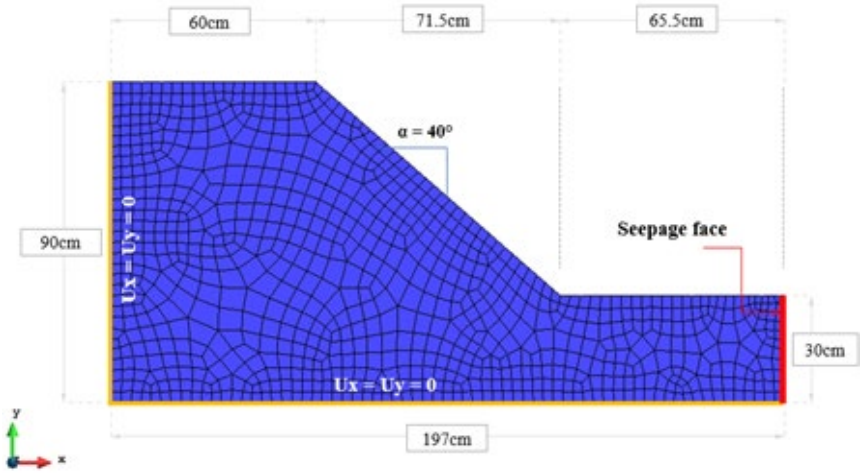

Figure 3. Geometry, hydraulic, and mechanical boundary conditions for the proposed numerical model.

Moreover, the simulations were performed in 2D with plane strain assumption. In order to study the effect of rainwater infiltration on slope stability, two numerical simulations were presented in this paper in Table 4.

Table 4. Reduced scale slope model characteristics, initial and boundary conditions.

Model type	Type of Test	Initial and boundary conditions	Rainfall period
A	Rainfall	Slope angle α = 40%, porosity n_0 = 0.471, saturation degree S_i = 30%, suction, s = 12.85kPa and rainfall intensity I = 50 mm/h	40000 sec
B	Rainfall	Slope angle α = 40%, porosity n_0 = 0.415, saturation degree S_i = 30%, suction s = 12.85kPa and rainfall intensity I = 50 mm/h	20000 sec

For the first test (Type A model as indicated in Table 4), the following figure shows the displacement and suction evolutions during the simulation and the obtained numerical results show that important displacements have occurred when the region near the toe of the slope becomes fully saturated. In addition, Fig. 4 confirms that important displacement (plastic deformation) occurred due the positive pore water pressure increase near the toe of the slope. Fig. 5 shows that the groundwater table begins to develop in the lower part of the slope and that the upper part remains unsaturated until the end of the simulation. On the other hand, Fig. 6 represents the positive pore water pressure isovalue at the end of the simulation. The obtained numerical results confirm that landslides occurred when the toe of the slope became saturated and positive pore water pressure developed. In our case, a superficial landslide occurred as shown in Fig. 7.

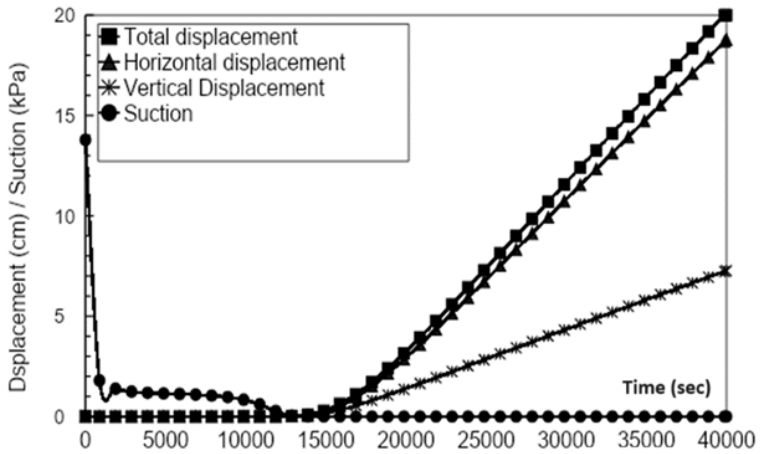

Figure 4. Displacement and suction against time for rainfall water infiltration.

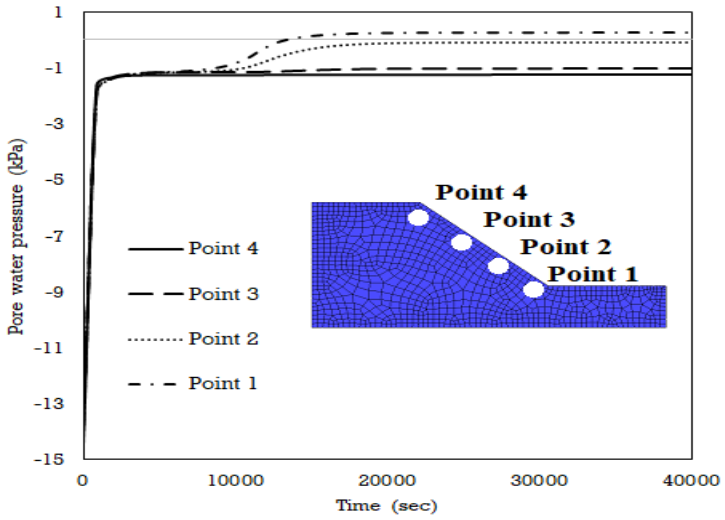

Figure 5. Pore water pressure in different points on the top layer of the slope.

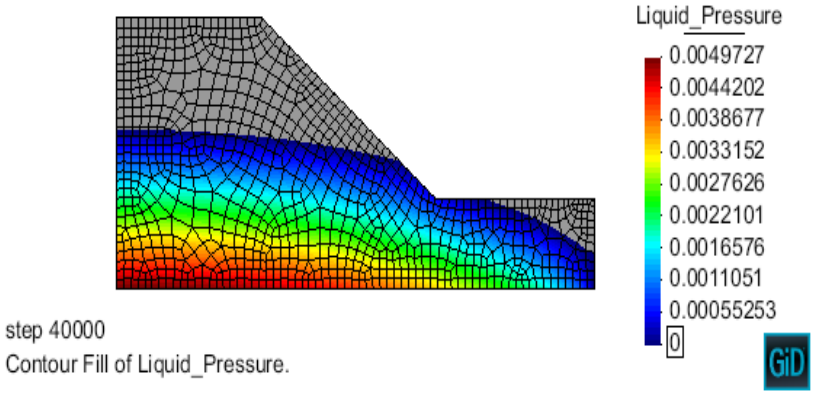

Figure 6. Positive pore water pressure isovalue at the end of infiltration period.

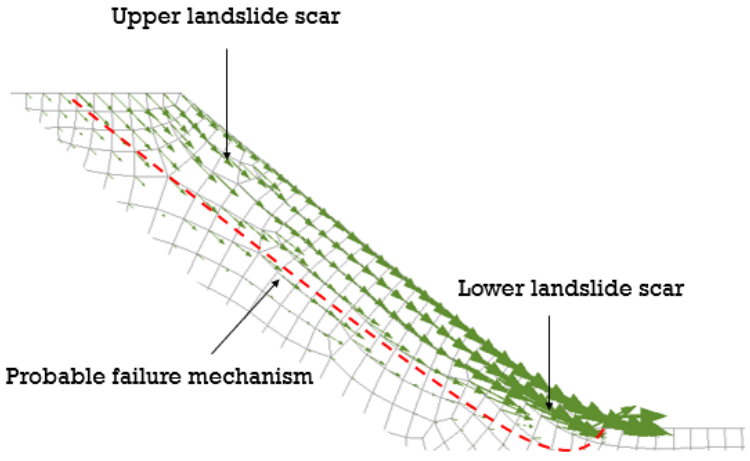

Figure 7. Vectors of incremental displacements at the end of rainwater infiltration.

In the second test, only the soil porosity and rainfall test duration were modified. Fig. 8 shows the numerical results of the vectors of incremental displacement and the contour of deviatoric plastic strain at the end of rainwater infiltration. The vectors of incremental displacements in Fig. 8 (a) delineate the most probable failure mechanism under current loading conditions. The consequences of rain infiltration on slope deformation are noticeable as the contours of accumulated deviatoric plastic strains ε_d^p in Fig. 8 (b) illustrate.

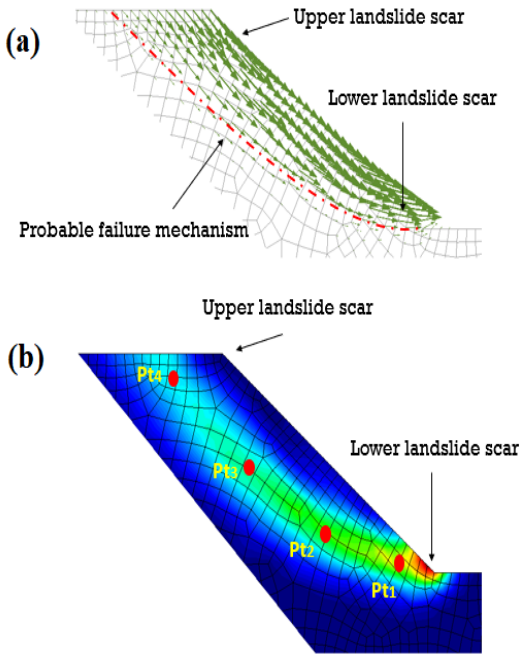

Figure 8. Vectors of incremental displacements and the contour of deviatoric plastic strains at the end of rainwater infiltration duration.

In this part of our simulation, an analysis of the temporal evolution of deviatoric plastic strains for different points located in the superficial layer of the slope allows identifying the most active shear zones during the water flow associated with the formation of a progressive failure mechanism (Fig. 9). Four different points, which are located in the shear zone identified in Fig. 8 (b), are selected for the analysis. At the beginning of rain infiltration, deviatoric plastic strain occurs in the shallow (Pt 1), lower part of the slope. Subsequently, plastic strain mobilized in the middle part (Pt 2) and finally in the upper part of the slope (Pts 3 and 4). As indicated, large irreversible shear strain occurred after 1200 sec of rainwater infiltration in the toe of the slope part. The most probable failure mechanism originates in the lower part of the slope, then the lower part is sheared and finally the shear zone spreads through the soil to the slope surface in the upper part.

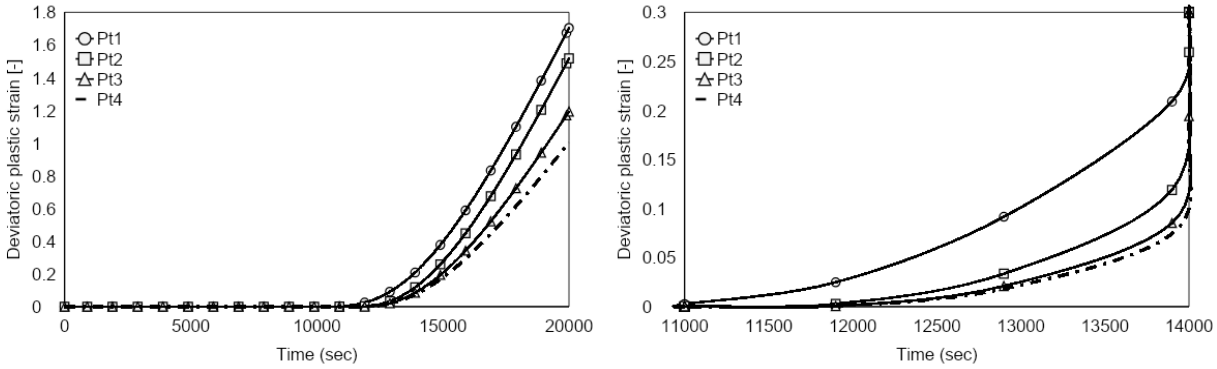

Figure 9. Evolution of deviatoric plastic strains in different superficial points.

4. Conclusions

Based on a current proposal of hydro-mechanical modeling, some conclusions can be given. Firstly, the introduced model modified Terzaghi's definition of the effective stresses by introducing parameter χ equal to the effective degree of saturation.

This means that the effective stresses change not only with water pressure, but also with the degree of saturation. The cohesion was formulated as a function of suction, and decreases along with suction. As a consequence, the soil shear strength decreases with the reduction in suction.

This model permitted the deformations calculation from the elastic state to plastic state until reaching the slope failure. This allowed us to analyze the progressive failure mechanism of one layer and multilayer slope.

In addition, we demonstrated that:

- The capillarity benefit was lost due to rainwater infiltration. Water infiltration led to an increase of pore water pressure (decrease of suction). The proposed numerical model also demonstrated its capability to correctly reproduce the pore water pressure distribution that triggers slope failure.
- The obtained numerical results show for the first time that rainwater infiltration leads to a loss in suction from the top slope layer. If the rainfall duration is long, the groundwater table level goes back up from the slope bottom. According to the analysis of plastic deformation in different parts of the slope, the failure mechanism originates in the lower part of the slope and the shear zone moves through the superficial part of the soil to the upper part of the slope. A large irreversible shear strain occurred, firstly in the toe of the slope due to the increase of pore water pressure and the decrease of the effective stress, and then a decrease in soil shear strength (which can be vanished in the extreme case) is considered as the main factor leading to the slope instability.
- The rainfall duration is a significant parameter for slope failure. The longer the duration is, the more rainwater infiltration happens. This induces local and shallow slope failure. If the duration is long, failure mass occurred more.
- The moved mass of soil is occurred according to a kinematic log-spiral line as it was proved for friction granular soils.
- Deviatory plastic strain is a main parameter used for failure assessment. Large deviatoric strain was reached in the failure zone (20 %) and the plastic irreversible strain started from 2 % to localize the beginning of a failure zone.
- When suction tends to zero (saturated zone), total and horizontal displacements increase suddenly.
- Using unsaturated hydraulic permeability and water retention curve, effective cohesion and friction as main data, the model has the capability to introduce different initial hydraulic and environmental conditions (wetting-drying cycles) and hydro-mechanical boundary conditions (wetting by raining, drying by evaporation and the mechanical loading).

References

1. Olivella, S., Jamei, M., Guiras, H., Hamouda, K. Ben, Hatira, M., Olivella, S. A study of the slope stability in unsaturated marly clay soil. Studia Geotechnica et Mechanica. 2008. XXX (1-2).
2. Jamei, M., Guiras, H., Olivella, S. Analysis of slope movement initiation induced by rainfall using the Elastoplastic Barcelona Basic Model. European Journal of Environmental and Civil Engineering. 2015. 19(9). Pp. 1033–1058. DOI: 10.1080/19648189.2014.996670
3. Lee, K., Suk, J., Kim, H., Jeong, S. Modeling of rainfall-induced landslides using a full-scale flume test. Landslides. 2021. 18(3). Pp. 1153–1162. DOI: 10.1007/s10346-020-01563-8
4. Batali, L., Andreea, C. Slope Stability Analysis Using the Unsaturated Stress Analysis. Case Study. Procedia Engineering. 2016. 143. Pp. 284–291. DOI: 10.1016/j.proeng.2016.06.036
5. Borja, R.I., Liu, X., White, J.A. Multiphysics hillslope processes triggering landslides. Acta Geotechnica. 2012. 7(4). Pp. 261–269. DOI: 10.1007/s11440-012-0175-6
6. Kakogiannou, E., Sanavia, L., Nicot, F., Darve, F., Schrefler, B.A. A porous media finite element approach for soil instability including the second-order work criterion. Acta Geotechnica. 2016. 11(4). Pp. 805–825. DOI: 10.1007/s11440-016-0473-5
7. Klubertanz, G., Bouchelaghem, F., Laloui, L., Vulliet, L. Miscible and immiscible multiphase flow in deformable porous media. Mathematical and Computer Modelling. 2003. 37(5–6). Pp. 571–582. DOI: 10.1016/S0895-7177(03)00050-5
8. Khalili, N., Geiser, F., Blight, G.E. Effective Stress in Unsaturated Soils: Review with New Evidence. International Journal of Geomechanics. 2004. 4(2). Pp. 115–126. DOI: 10.1061/(asce)1532-3641(2004)4:2(115)
9. Qi, S., Vanapalli, S.K. Simulating Hydraulic and Mechanical Responses of Unsaturated Expansive Soil Slope to Rainfall: Case Study. International Journal of Geomechanics. 2018. 18(6). Pp. 1–17. DOI: 10.1061/(asce)gm.1943-5622.0001106
10. Rahimi, A., Rahardjo, H., Leong, E.C. Effect of hydraulic properties of soil on rainfall-induced slope failure. Engineering Geology. 2010. 114(3–4). Pp. 135–143. DOI: 10.1016/j.enggeo.2010.04.010
11. Sanavia, L. Numerical modelling of a slope stability test by means of porous media mechanics. Engineering Computations (Swansea, Wales). 2009. 26(3). Pp. 245–266. DOI: 10.1108/02644400910943608
12. Chen, P., Lu, N., Formetta, G., Godt, J.W., Wayllace, A. Tropical Storm-Induced Landslide Potential Using Combined Field Monitoring and Numerical Modeling. Journal of Geotechnical and Geoenvironmental Engineering. 2018. 144(11). DOI: 10.1061/(asce)gt.1943-5606.0001969
13. Karube, D., Kawai, K. The role of pore water in the mechanical behavior of unsaturated soils. Geotechnical and Geological Engineering. 2001. 19(3–4). Pp. 211–241. DOI: 10.1023/A:1013188200053
14. Pham, K., Lee, H., Kim, D., Lee, I.M., Choi, H. Influence of hydraulic characteristics on stability of unsaturated slope under transient seepage conditions. Landslides. 2018. 15(9). Pp. 1787–1799. DOI: 10.1007/s10346-018-0989-x
15. Pham, K., Kim, D., Choi, H.J., Lee, I.M., Choi, H. A numerical framework for infinite slope stability analysis under transient unsaturated seepage conditions. Engineering Geology. 2018. 243. Pp. 36–49. DOI: 10.1016/j.enggeo.2018.05.021
16. Ran, Q., Hong, Y., Li, W., Gao, J. A modelling study of rainfall-induced shallow landslide mechanisms under different rainfall characteristics. Journal of Hydrology. 2018. 563. Pp. 790–801. DOI: 10.1016/j.jhydrol.2018.06.040.

17. Hamrouni, F., Trabelsi, H., Jamei, M. Numerical Analysis of the Drilled Horizontal Drains Efficiency in Physical Slope Model: The Role of the Soil Water Retention Property. Geotechnical and Geological Engineering. 2022. 40(1). Pp. 195–211. DOI: 10.1007/s10706-021-01894-w
18. Hamrouni, F., Trabelsi, H., Jamei, M., Olivella, S. Numerical analysis of landslides caused by rainfall in a reduced physical slope model. European Journal of Environmental and Civil Engineering. 2019. DOI: 10.1080/19648189.2019.1580223
19. Kim, J., Kim, Y., Jeong, S., Hong, M. Rainfall-induced landslides by deficit field matric suction in unsaturated soil slopes. Environmental Earth Sciences. 2017. 76(23). Pp. 1–17. DOI: 10.1007/s12665-017-7127-2
20. Orense, R.P., Shimoma, S., Maeda, K., Towhata, I. Instrumented Model Slope Failure due to Water Seepage. Journal of Natural Disaster Science. 2004. 26(1). Pp. 15–26. DOI: 10.2328/jnds.26.15
21. Chueasamat, A., Hori, T., Saito, H., Sato, T., Kohgo, Y. Experimental tests of slope failure due to rainfalls using 1g physical slope models. Soils and Foundations. 2018. 58(2). Pp. 290–305. DOI: 10.1016/j.sandf.2018.02.003
22. Orense, R.P. Slope Failures Triggered by Heavy Rainfall. Philippine Engineering Journal Pej. 2004. 25(2). Pp. 73–90.
23. Damiano, E., Olivares, L. The role of infiltration processes in steep slope stability of pyroclastic granular soils: Laboratory and numerical investigation. Natural Hazards. 2010. 52(2). Pp. 329–350. DOI: 10.1007/s11069-009-9374-3
24. Hakro, M.R., Harahap, I.S.H. Laboratory experiments on rainfall-induced flowslide from pore pressure and moisture content measurements. Natural Hazards and Earth System Sciences Discussions. 2015. 3(2). Pp. 1575–1613. DOI: 10.5194/nhessd-3-1575-2015
25. Yan, J. fan, Shi, B., Ansari, F., Zhu, H. hu, Song, Z. pu, Nazarian, E. Analysis of the strain process of soil slope model during infiltration using BOTDA. Bulletin of Engineering Geology and the Environment. 2017. 76(3). Pp. 947–959. DOI: 10.1007/s10064-016-0916-0
26. Ling, H., Ling, H.I. Centrifuge Model Simulations of Rainfall-Induced Slope Instability. Journal of Geotechnical and Geoenvironmental Engineering. 2012. 138(9). Pp. 1151–1157. DOI: 10.1061/(asce)gt.1943-5606.0000679
27. Montrasio, L., Valentino, R. A model for triggering mechanisms of shallow landslides. Natural Hazards and Earth System Science. 2008. 8(5). Pp. 1149–1159. DOI: 10.5194/nhess-8-1149-2008
28. Montrasio, L., Schilirò, L., Terrone, A. Physical and numerical modelling of shallow landslides. Landslides. 2016. 13(5). Pp. 873–883. DOI: 10.1007/s10346-015-0642-x
29. Sasahara, K., Sakai, N. Development of shear deformation due to the increase of pore pressure in a sandy model slope during rainfall. Engineering Geology. 2014. 170. Pp. 43–51. DOI: 10.1016/j.enggeo.2013.12.005.
30. Olivella, S., Gens, A., Carrera, J., Alonso, E.E. Numerical formulation for a simulator (CODE_BRIGHT) for the coupled analysis of saline media. Engineering Computations (Swansea, Wales). 1996. 13(7). Pp. 87–112. DOI: 10.1108/02644409610151575
31. Laloui, L., Nuth, M. On the use of the generalised effective stress in the constitutive modelling of unsaturated soils. Computers and Geotechnics. 2009. 36(1–2). Pp. 20–23. DOI: 10.1016/j.compgeo.2008.03.002
32. Lu, N., Khalili, N., Nikooee, E., Hassanizadeh, S.M. Principle of Effective Stress in Variably Saturated Porous Media. Vadose Zone Journal. 2014. 13(5). Pp. vzj2014.04.0038. DOI: 10.2136/vzj2014.04.0038
33. Lu, N., Godt, J.W., Wu, D.T. A closed-form equation for effective stress in unsaturated soil. Water Resources Research. 2010. 46(5). Pp. 1–14. DOI: 10.1029/2009wr008646
34. Ali, T., Showkat, R., Babu, G.L.S. Hydro-Mechanical Simulations of Unsaturated Soil Slope. Indian Geotechnical Journal. 2021. 51(4). Pp. 861–869. DOI: 10.1007/s40098-021-00554-3
35. Fredlund, D.G., Vanapalli, S.K., Rahardjo, H. Use of linear and nonlinear shear strength versus matric suction relations in slope stability analyses. Landslides; proceedings of the sixth international symposium. 1992. 6 (January 2021). Pp. 531–537.
36. Fredlund, D.G., Vanapalli, S.K. Shear Strength of Unsaturated Soils. Methods of Soil Analysis, Part 4: Physical Methods. 2018. 321. Pp. 329–361. DOI: 10.2136/sssabookser5.4.c15
37. Lu, N., Likos, W.J. Suction Stress Characteristic Curve for Unsaturated Soil. Journal of Geotechnical and Geoenvironmental Engineering. 2006. 132(2). Pp. 131–142. DOI: 10.1061/(asce)1090-0241(2006)132:2(131)
38. Zhang, L.L., Fredlund, D.G., Fredlund, M.D., Ward Wilson, G. Modeling the unsaturated soil zone in slope stability analysis. Canadian Geotechnical Journal. 2013. 51(12). Pp. 1384–1398. DOI: 10.1139/cgj-2013-0394
39. Zeng, F., Li, Y., Labuz, J.F. Paul-Mohr-Coulomb Failure Criterion for Geomaterials. Journal of Geotechnical and Geoenvironmental Engineering. 2018. 144(2). Pp. 1–5. DOI: 10.1061/(asce)gt.1943-5606.0001829
40. Damiano, E., Olivares, L., Picarelli, L. Steep-slope monitoring in unsaturated pyroclastic soils. Engineering Geology. 2012. 137–138. Pp. 1–12. DOI: 10.1016/j.enggeo.2012.03.002
41. Mualem, Y. Hydraulic conductivity of unsaturated porous media: Generalized macroscopic approach. Water Resources Research. 1978. 14(2). Pp. 325–334. DOI: 10.1029/WR014i002p00325
42. Genuchten, V.M. A closed-form equation for predicting the hydraulic conductivity of unsaturated soils. Soil Science Society of America Journal. 1980. 44(5). Pp. 892–898.
43. Mualem, Y. A new model for predicting the hydraulic conduc. Water Resources Research. 1976. 12(3). Pp. 513–522.
44. Vaunat, J., Nord, C. Code _ Bright / Gid : a 3-D Program for Thermo-Hydro-Mechanical Analysis in. Pp. 3–6.

Information about authors:

Facker Hamrouni,
ORCID: https://orcid.org/0000-0002-6165-2550
E-mail: fakher.hamrouni@gmail.com

Mehrez Jamei, *Doctor of Science*
ORCID: https://orcid.org/0000-0002-9430-3920
E-mail: mehjamei@yahoo.fr

Yahya Alassaf, *PhD*
ORCID: https://orcid.org/0000-0002-9430-3920
E-mail: yahya.alassaf@nbu.edu.sa

Received 24.05.2022. Approved after reviewing 09.01.2023. Accepted 16.01.2023.